Influence of wall heterogeneity on nanoscopically confined polymers†

Raffaele Pastore,*[a,b,c] Alessio David,[c] Mosè Casalegno,[c] Francesco Greco,[a] and Guido Raos*[c]

We investigate via molecular dynamics simulations the behavior of a polymer melt confined between surfaces with increasing spatial correlation (patchiness) of weakly and strongly interacting sites. Beyond a critical patchiness, find a dramatic dynamic decoupling, characterized by a steep growth of the longest relaxation time and a constant diffusion coefficient. This arises from dynamic heterogeneities induced by the walls in the adjacent polymer layers, leading to the coexistence of fast and slow chain populations. Structural variations are also present, but they are not easy to detect. Our work opens the way to a better understanding of adhesion, friction, rubber reinforcement by fillers, and many other open issues involving the dynamics of polymeric materials on rough, chemically heterogeneous and possibly "dirty" surfaces.

1 Introduction

The dynamics of polymers near solid surfaces or in nanoscopically confined environments has come under intense scrutiny in recent years. Indeed, many practical problems such as polymer-mediated adhesion,[1] lubrication and friction[2,3], micro- and nano-fluidics,[4,5] deposition of thin films,[6] processing of polymer nanocomposites and rubber reinforcement by fillers[7–11] involve the motion, deformation and relaxation of macromolecules on one or between two close surfaces. Many experimental, theoretical and computational studies have demonstrated that the behavior of polymers in these situations may deviate very significantly from that in the bulk. Examples of such deviations in the dynamical properties include the glass transition[12–14] and the diffusivity of polymers in nanocomposites and in narrow slits.[15,16] Important insights have been obtained by studying simple, well-defined model systems, such as polymers sandwiched between smooth, homogeneous surfaces.[17] On the other hand, the applications mentioned above often involve the interaction of polymers with rough, chemically heterogeneous and possibly "ill-defined" surfaces and nanoparticles. A classic example is carbon black, which is widely applied in rubber reinforcement and is known to have a strongly heterogeneous surface topography and chemistry.[18,19]

Theoretical and computational studies of single chains on heterogeneous surfaces have shown that both spatial and energetic disorder (i.e., roughness and chemical heterogeneity, respectively) can be very important, enhancing the polymer absorption in comparison to the reference homogeneous case.[7,20] The absorption transition is accompanied by an entropic reduction, which is compensated by an energetic gain: the chain may adopt a flat "pancake" conformation in order to optimize its interaction with the more strongly absorbing sites. This has important consequences also for the chain dynamics, leading to a slowing-down and possibly a structural arrest analogous to the glass transitions.[21] While these results are quite appealing and suggestive, the single-chain behavior cannot be directly traslated to homopolymer melts. When a surface consists of patches of strongly and weakly absorbing regions, a single chain will preferentially absorb on the former, while in the case of polymer melts some chains will necessarily cover the latter. Also, there is little incentive for a particular chain to localize or adapt its conformation in order to maximize its interaction with the strongly absorbing sites/patches: this would require the displacement of other chains, with poor energetic compensation for single-chain entropy reduction. Such differences lead us to expect rather different physics for single chains and melts. The latter is the main focus of this work.

In the past, theory and computer simulation (Monte Carlo or Molecular Dynamics, MD) have been applied extensively to the investigation of polymers near or between homogeneous surfaces.[22–28] Our group has addressed the role of surface disor-

[a] Department of Chemical, Materials and Production Engineering, University of Naples Federico II, P.le Tecchio 80, Napoli 80125, Italy.

[b] CNR-SPIN, Via Cintia, 80126 Napoli, Italy.

[c] Dipartimento di Chimica, Materiali e Ingegneria Chimica G. Natta, Politecnico di Milano, via L. Mancinelli 7, 20131 Milano, Italy.

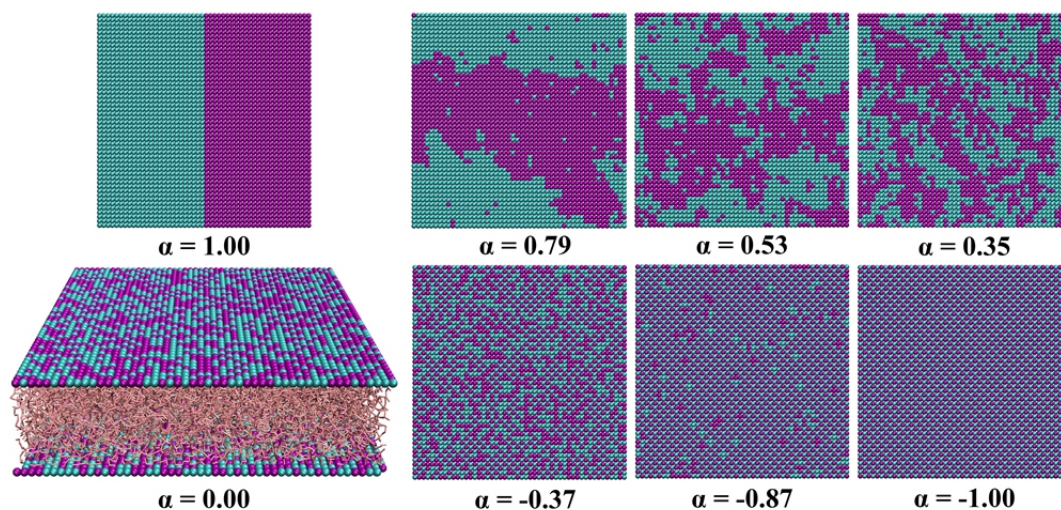* Corresponding authors: raffaele.pastore@unina.it, guido.raos@polimi.it.

Fig. 1 Investigated model system. Illustration of surfaces at different values of α, as indicated. The whole system is shown for a single example ($\alpha = 0$).

der and heterogeneities by simulating and analyzing the dynamics of a polymer monolayer on a surface consisting of random mixtures of weakly and strongly interacting sites in variable proportion.[29–31] Despite of the simplicity of the model, we found significant effects, such as a non-monotonic dependence of lateral polymer mobility on surface composition and the onset of Fickian yet not Gaussian diffusion[32]. Here we introduce a new model, by considering a homopolymer melt nanoscopically confined between two surfaces with variable and controllable degrees of "patchiness".

Fig.1 contains sketches of the investigated systems (see the next Section for details). A bead-and-spring polymer is confined between two parallel surfaces. The chains consist of $N=32$ identical P-type beads (P stands for polymer). The polymer has a constant, bulk-like density at the center of the film. The relatively small size of the chains prevents the formation of an appreciable number of "bridges" from one surface to the other. Also, the combination of temperature (much higher than the bulk glass transition temperature) and chain length (lower than the entanglement length) is such that the polymer would display Rouse-like dynamics[33,34] in the absence of the walls. The surfaces are made up of a 50:50 mixture of weakly-interacting (W) and strongly interacting (S) beads. A parameter α varies in the range $[-1,+1]$ and describes situations where W and S beads are *i)* prevalently intermixed ($\alpha < 0$), *ii)* randomly distributed ($\alpha = 0$), or *iii)* tend to cluster and thus to form "patchy" surfaces ($\alpha > 0$). By doing so, the average extension of the heterogeneities increases systematically from being well below to well above the characteristic chain size. We purposely did not vary the chain length, so as to preserve the degree of confinement of the systems and avoid the transition to an entangled regime.

The picture emerging from our results is that, by random yet proper functionalization of the solid walls, it is possible to modulate greatly their dynamic and mechanical effects on nanoscopically confined polymers, with minor structural modifications.

2   Models and Methods

MD simulations. We have simulated the dynamics of a generic bead-and-spring model of a polymer melt, confined between two parallel surfaces characterized by tunable spatial correlations in their chemical composition. The sites making up the surfaces are either weakly (W) or strongly (S) interacting. The surface as well as the polymer beads have identical diameters, as specified by the Lennard-Jones (LJ) parameter $\sigma = 1$. In these distance units, the surfaces are located at $z=0.0$ and $z=13.0$, and the unperturbed root-mean-square radius of gyration of the chains in the bulk is $R_g = 2.65$.

All pairwise non-bonded interactions are described by truncated and force-shifted LJ potentials:

$$V_{PQ}^{LJ}(r) = 4\varepsilon_{PQ}[(\sigma/r)^{12} - (\sigma/r)^6] - V_{PQ}^{cut}(r) \qquad (1)$$

if $r < r_{cut}$, $V_{PQ}^{LJ}(r) = 0$ otherwise. Here the uppercase subscripts indicate the type of particles (i.e., P, W or S), ε_{PQ} is the interaction strength (LJ well depth), $r_{cut} = 2.5\sigma$ is the cutoff distance, and $V_{PQ}^{cut}(r)$ is a linear function which zeroes for the potential and the force at the cutoff, thus preserving their continuity. The interaction strength between polymer beads is $\varepsilon_{PP} = \varepsilon$. The W and S surface sites differ by their interaction energy with the polymer beads, which are respectively equal to $\varepsilon_{PW} = \varepsilon$ and $\varepsilon_{PS} = 4\varepsilon$. With this choice, we intentionally focus on a case with marked difference between S and W sites. A 4:1 ratio between P-S and P-W interactions is reasonable as it is comparable to that between the strongest and weakest interactions in the coarse-grained MARTINI force field.[35].

The bonded interactions within a polymer are modeled by the sum of a LJ potential analogous to Eq.(1) and a finitely extensible nonlinear elastic spring (FENE):

$$U_{FENE}(r) = 0.5 \ k \ R_0^2 \ln[1 - (r/R_0)^2] \qquad (2)$$

where $k = 30\varepsilon/\sigma^2$ is the force constant and $R_0 = 1.3\sigma$ is the max-

imum extensibility of the bonds. [36] The reduced R_0 value (in the standard Kremer-Grest model [37] $R_0 = 1.5\sigma$) decreases the equilibrium bond length to $r = 0.79$, creating a mismatch between the bonded and non-bonded nearest-neighbor distances. This reduces the tendency of the polymer to order and possibly crystallize at a flat interface—an effect which is overestimated by many simple coarse-grained models.

The fraction of S sites is fixed at $f = 0.5$ (i.e., the 50%-50% composition), unlike in our previous work [30,31] where f was varied over the whole [0,1] range but the sites' arrangement was completely random. Here instead we model situations with different degrees and types of order in the surfaces, as described below. Units are reduced so that $\sigma = m = \varepsilon = k_B = 1$, where m is the mass of all beads and k_B is the Boltzman constant. The system contains 1000 polymer chains of length $N=32$ (37000 beads, including the surfaces). The polymer bead number density at the center of the slab is about 1.05, which corresponds to the equilibrium value for the bulk system at zero applied pressure (the pure polymer system was also simulated, for comparison). Periodic boundary conditions were adopted in all directions (in the slab simulations, the simulation box has length 14 in the z directions, so that the upper wall is one unit distance below the periodic image of the lower one). The production runs were performed in the NVT ensemble, using a Nose-Hoover thermostat and the velocity-Verlet algorithm to integrate the equations of motion, as implemented in LAMMPS. [38] Data were acquired after carefully equilibrating the systems at temperature $T = 1$.

Surface models. The surface sites are arranged in a square-planar configuration, with a lateral extension of 50×50 (with periodic boundary conditions) and an areal number density of 1.0. Eight different types of surfaces, corresponding to different degrees of patchiness or intermixing of the W and S sites have been produced by spin-interchange Monte Carlo simulations of a two-dimensional Ising-type model [39]. The generated morphology depends of the type of coupling between nearest-neighbor "spins" (ferromagnetic or antiferromagnetic) and on the reduced temperature T^* employed in the Monte Carlo simulation. For each disordered surface model, the upper surface is generated independently of the lower one.

We have characterized the short-range order of the surfaces thus generated by the Warren-Cowley order parameter for a binary mixture [40]:

$$\alpha^{(I)} = 1 - \frac{n_{IJ}}{x_I(n_{II} + n_{IJ})} \qquad (I \neq J = W, S) \qquad (3)$$

where x_I is the fraction of sites of type I, and n_{IJ} is the average number of J-type nearest-neighbors to an I-type site. This general definition simplifies in our case because $x_W = x_S = 0.5$, $n_{SW} = n_{WS}$ and $n_{SS} = n_{WW}$ (compositional symmetry of the surfaces) and $n_{WW} + n_{WS} = n_{SS} + n_{SW} = 4$ (four-fold coordination of the square lattice). Thus there is a single α parameter, and we will use it without the superscript. A positive value indicates some segregation with a tendency of the surface sites to be surrounded by like-type sites, while a negative value indicates intimate intermixing with a tendency of the W sites to be surrounded by S sites, and vice versa. The values $\alpha = +0.96$, 0.79, 0.53, 0.35 were

obtained from the ferromagnetic model at increasing temperatures ($T^*=0.0$, 2.0, 2.5 and 3.3, respectively) while $\alpha = -0.37$, -0.86 and -1.00 were obtained from the antiferromagnetic version of the model ($T^*=3.3$, 2.0 and 0.0, respectively). The $\alpha = 0.00$ case corresponds to the surface with completely random intermixing of W and S sites ($T^* = \infty$). We have used these α values when discussing systems' behavior as a function of surface morphology, with the exception of $\alpha = +0.96$ which has been approximated to 1.00 for simplicity.
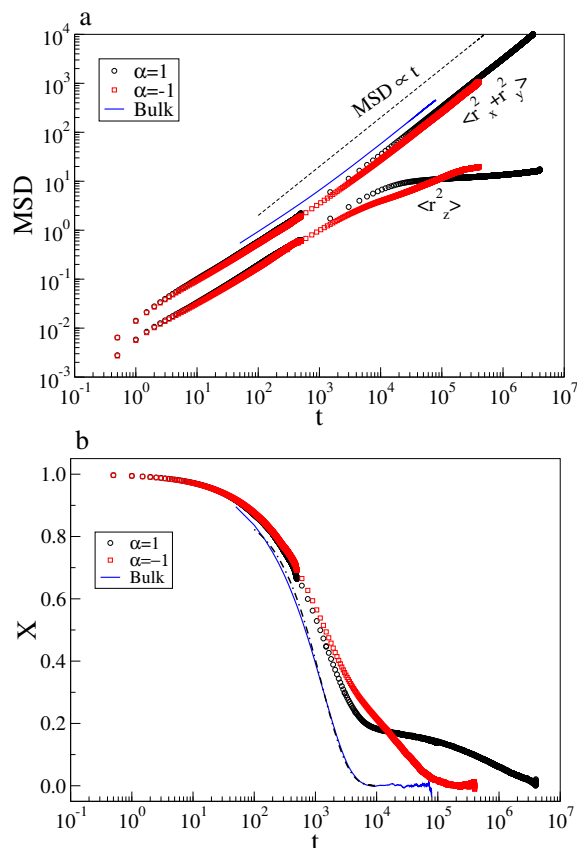

Fig. 2 Mean square displacement (MSD) and Autocorrelation of the chain end-to-end vector (EEVA). For the systems with $\alpha = 1$ and -1: a) MSD as a function of time along the vertical/confined directions and in the horizontal/unconfined plane, as indicated. For comparison, this latter is also reported for the bulk system, where all directions are statistically equivalent. The dashed line is a guide to the eye, corresponding to ordinary diffusion, MSD$\propto t$. b) EEVA, X, as a function of time. EEVA of the bulk system is also reported and well fitted by a simple exponential, $X(t) \propto e^{-t/\tau}$, (dashed line).

3 Results

Dynamics - We start by discussing the behavior of global dynamic quantities, i.e. averages are computed over all system chains as well as over different time origins. To illustrate the impact of surface heterogeneities on the polymer dynamics, we first focus on the systems with largest and smallest degrees of patchiness, $\alpha = 1$ and $\alpha = -1$, and make comparison with the reference bulk

system.

Fig.2a shows the mean-square displacements (MSDs) of the centre-of-mass of the chains along the unconfined/horizontal directions and the confined/vertical one, $\langle r_x^2(t) + r_y^2(t)\rangle$ and $\langle r_z^2(t)\rangle$. The MSDs increase with a slightly non-diffusive behaviour in the short time limit. On longer timescale, the z component saturates due to confinement. Conversely, the horizontal component fully attains the diffusive regime, showing a behavior qualitatively similar to the bulk system, but with a smaller diffusion coefficient, in agreement with previous results[23]. More importantly, it is apparent that horizontal diffusion is hardly affected by surface topography, as the MSDs relative to $\alpha = 1$ and $\alpha = -1$ are almost overlapped, the former being only slightly larger than the latter.

The autocorrelation of the chain end-to-end vector (EEVA), $X(t) = \langle R(0)R(t)\rangle/\langle R(0)\rangle^2$, provides a complementary perspective on the polymer dynamics. In a bulk polymer liquid, the relaxation of this intramolecular quantity requires a time comparable to that for the diffusion of the macromolecule by a distance comparable to its radius of gyration.[33] The present situation is different. Fig.2b shows that both confinement and surface morphology have a clear impact on the decay of $X(t)$, producing important qualitative changes to it. Indeed, a single exponential decay fully describes the bulk data, whereas the confined systems clearly deviate from it. The $X(t)$ of the two confined systems overlap at short times but decouple at intermediate ones, the $\alpha = -1$ data decreasing more slowly. This trend reverses at late times, giving rise to an intriguing crossing of the two curves. Thus, the system with faster intermediate time dynamics ($\alpha = 1$) displays the slower long-time relaxation. We checked that, considering all the α values in $[-1,1]$, there is a gradual transition between the two extreme behaviors presented in Fig.2. We note as an aside that the horizontal and the vertical components of the EEVA do not show remarkable differences in their decay (see Fig. ESI1 in the ESI†). We also signal that the autocorrelation of the first Rouse normal mode behaves, as expected, very similarly to the EEVA.

In order to quantify these features, we measured (a) the diffusion coefficient D from a linear fit to the long-time data of the horizontal MSD component, $\langle r_x^2(t) + r_y^2(t)\rangle \simeq 4Dt$, and (b) the relaxation time τ_l characterizing the late decay of $X(t)$. In order to measure τ_l, we adopted an exponential fit $X(t) \simeq A_l e^{-t/\tau_l}$ that, if limited to long times, effectively describes the data for all confined systems (see Fig. ESI2 in the ESI†). Fig.3a compares the diffusion times $\tau_D = R_g^2/4D$ (where R_g corresponds to the bulk value given above) and the longest relaxation times τ_l. Their different dependence on the patchiness parameter α highlights a clear decoupling. Indeed, while τ_D is essentially flat, τ_l rapidly increases by almost two orders of magnitude when α enters the [0.5,1.0] range.

A decoupling between the self-diffusion coefficient and the structural relaxation time is commonly observed in molecular and colloidal glass–forming liquids on lowering the temperature and increasing the volume fraction, respectively,[41–45] eventually leading to a spectacular breakdown of the Stokes-Einstein relation[46–48]. In those systems, the decoupling is ascribed to the presence of Dynamic Heterogeneities (DHs), namely, a broad mobility distribution accompanied by some clustering of fast and
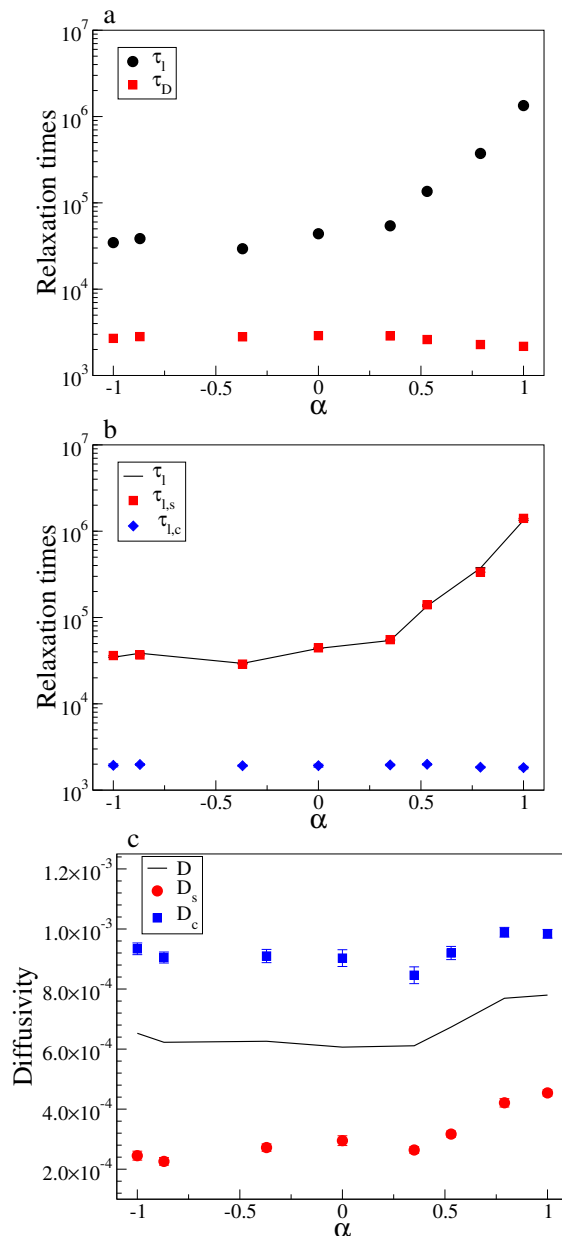

Fig. 3 Dynamic Decoupling. α dependence of a) diffusion time τ_D and EEVA longest relaxation time τ_l, computed over the overall system, b) EEVA z-resolved longest relaxation times, $\tau_{l,c}$ and $\tau_{l,s}$, and c) diffusion coefficients, D_c and D_s, as computed in a central slab and in a slab close to the surface, respectively. For a direct comparison, the corresponding global quantities, τ_l and D, are also reported in panels b) and c), respectively.

slow particles[49–51]. The diffusion coefficient is dominated by the fast particles and the structural relaxation time by the slow ones[41,52,53]. It is also worth noticing, incidentally, that identifying a clear structural origin for DHs in glass forming liquids is a long standing and still unsolved issue.[54]

We now show that DHs are indeed present in our systems and are triggered by the confining walls. To prove this, we partitioned the system into four slices along the z direction and monitored the MSD and the EEVA of chains initially "belonging" to differ-

ent slices. Notice that, with this partition, the thickness of the slices (=13.0/4) is similar to the average chain radius of gyration. The statistical equivalence of the two near-wall and the two central slices enables further averaging over each pair. Using this approach, we measured the z-resolved late relaxation times, $\tau_{l,s}$ and $\tau_{l,c}$, and diffusion coefficients, D_s and D_c (subscripts c and s indicate quantities measured at the center or close to the surfaces, respectively). Fig.3b shows that, on changing α, $\tau_{l,s}$ closely mimics the behavior of the longest relaxation time of the overall system. Instead, the central relaxation time, $\tau_{l,c}$, is much smaller than $\tau_{l,s}$ (up to two orders of magnitude), and independent of the surface morphology. As regards the diffusion coefficients, Fig.3c shows that $D_c \simeq 4D_s$, both quantities being roughly independent of α. The global diffusion coefficient lies between D_c and D_s, being slightly closer to the former.

These results strongly support the coexistence of slow and fast chains. The slowest chains, in fact controlling the global relaxation time τ_l, are those close to the surfaces. The slowing-down of the dynamics, which becomes dramatic when $\alpha \geq 0.5$, can likely be ascribed to the presence of chains mainly adsorbed on patches of strongly attractive sites. Indeed, these *strongly adsorbed chains* show up and proliferate when the average patch size becomes comparable and progressively overcomes the chain gyration radius. Under the same condition ($\alpha \geq 0.5$), of course, there is also a complementary population of chains mainly adsorbed on weakly attractive sites. These *weakly adsorbed chains* should have a larger mobility compared to the strongly adsorbed ones and control the surface diffusivity. Indeed, D_s is slightly smaller than D_c, even if $\tau_{l,s}$ is much larger than $\tau_{l,c}$. Finally, the fast chains control the global diffusivity, D. The high, nearly α-independent values of D_c confirm that these are mostly concentrated in the centre of the slab. However, since D_s is not so much smaller than D_c, also the weakly absorbed chains contribute to the global D and determine its dependence on surface morphology.

The z-resolved analysis of the dynamics also leads to a clear rationalization of the crossing of the EEVA curves in Fig. 2. The early-time decay is insensitive to the type of surface, being due to the relaxation of the chains at the center. Later on, the decay becomes α-dependent as it is due to the relaxation of the chains close to the walls. When $\alpha = 1$, the intermediate- and long-time EEVA decays are controlled by the relaxation of the weakly and the strongly adsorbed chains, respectively. Conversely, when the surface inhomogeneities are smaller than R_g ($\alpha = -1$), all the adsorbed chains experience the same average interaction with the walls and relax at a comparable, intermediate rate.

Structure - According to common expectations, some structural variations within the polymer melt should accompany the α-dependent changes in chain dynamics. In order to spot such structural features, we start by showing in Fig.4a and b one configuration of the polymer beads within the first two thin layers, on top of an $\alpha = 1$ surface (see Fig. ESI3 in the ESI†for the $\alpha = -1$ case). It is apparent that the density in the second layer is smaller than in the first one, in agreement with the well-known density oscillations occurring even next to a homogeneous wall over a few bead diameters. [22] Here it is more interesting to focus on the structural changes in the horizontal plane, as these should depend on wall morphology. These changes are clearly visible in the first layer (panel a): the left part, overlapped to S sites, is both denser and more ordered than the right one, overlapped to W sites. Since these signatures already appear to be obliterated in the second layer, it seems worth concentrating on the structure of the very first layer. Interestingly, the pair distribution functions calculated between the polymer beads belonging to first layers are fairly insensitive to α (see Fig. ESI4 in the ESI†). Instead, we observe some differences in the histograms of the coordination numbers (Fig.4c). These were computed by counting the neighbors of the polymer beads up to a cutoff of 1.4, excluding surface sites. The distribution for $\alpha = 1$ is broader than for $\alpha = -1$, with an appreciably larger probability of the lowest coordination numbers. This indicates a more heterogeneous structure and, therefore, a more heterogeneous segment-level dynamics on increasing the surface patchiness. However, a connection with the growth of τ_l is not straightforward at this stage. Further insights come from the histograms of the polymer-wall interaction energies, as computed by the sum of the individual P-W and P-S non-bonded interactions, and shown in Fig.4d. Indeed, the broader distribution in the $\alpha = 1$ case, with a fatter and longer tail on the strong side of the energy range, directly supports the presence of *strongly adsorbed chains*, justifying the growth of τ_l at large α values.

At this point in the discussion, it should be clear that by focusing on the distributions of local quantities, and especially on their tails, it is possible to unveil structural changes with α, even though these may seem to be minor in comparison with those in the chain dynamics. Now we ask whether some changes are detectable also in average structural quantities, which are more commonly and feasibly measured in experiments. Fig.5a shows that the average polymer-wall interaction energy, as computed from distributions like those in Fig.4d, is, in fact, insensitive to the value of α. Note that the "error bars" in the plot represent the standard deviations of the associated distributions and, therefore, they simply indicate that a chain can be found in a range of different energetic environments. Fig.5b shows the perpendicular and parallel components of the chains' radii of gyration, measured within the same z-layers already adopted for the chain dynamics. The figure demonstrates that the walls produce a "squeezing" in the chains' conformation, $R_{\parallel s}^2 \simeq 3R_{\perp s}^2$, in comparison with the more isotropic conformations in the central slab, $R_{\perp c}^2 \simeq R_{\parallel c}^2$. This situation is illustrated by the insets 5c and d, showing the configuration of two chains in the middle of the system and close to a surface. However, also in this case there is no dependence of those chain properties on wall morphology. These results confirm that average structural quantities, even if z-resolved, may not display a dependence on the wall heterogeneities. On averaging, the structural features of the *strongly adsorbed chains* are likely balanced by those of the *weakly adsorbed chains*.

4 Discussion and Conclusions

Our simulations of confined polymer melts indicate that the presence of structured attractive walls triggers a global slow-down of the polymer dynamics with gradients along the z direction. More importantly, we find that spatial correlations in the surface com-
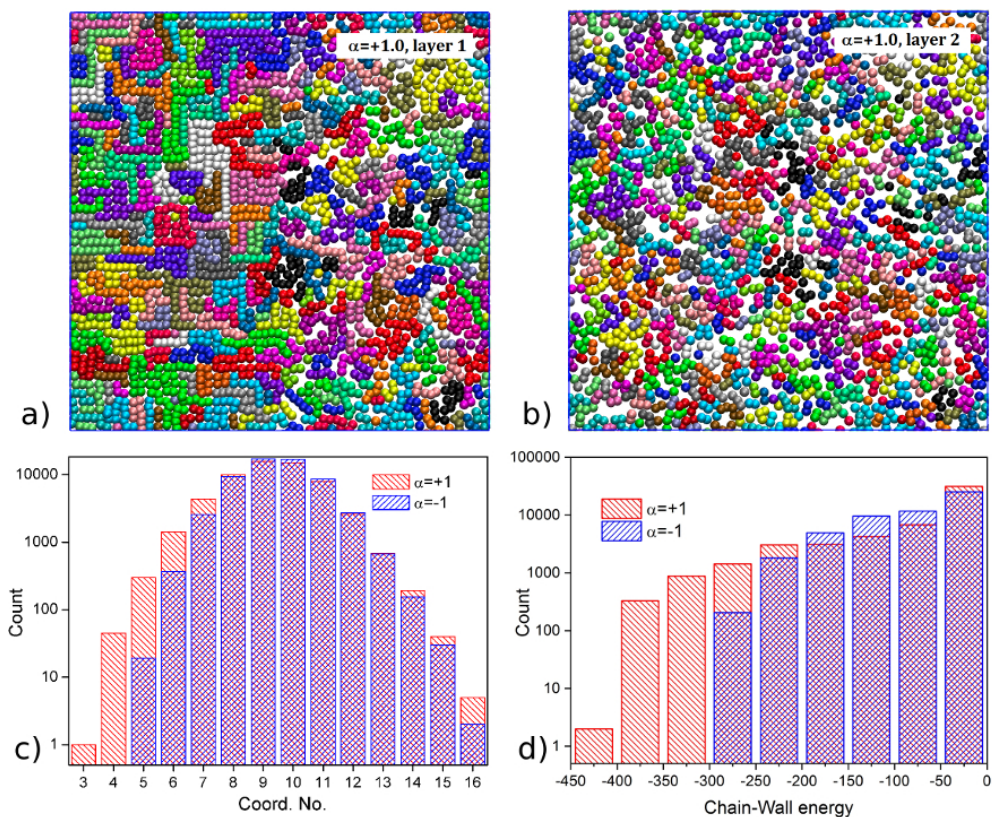
Fig. 4 Finely resolved structural properties. (a) Snapshot of the first polymer layer ($0.6 < z \leq 1.4$), on the $\alpha = +1$ surface. Polymer beads belonging to the same chain are represented with the same color. The S stripe is on the left-hand side, the W stripe on the right-hand one. (b) Same as (a), for the second layer ($1.4 < z \leq 2.2$). (c) Histograms of the coordination numbers of the polymer beads (cutoff at $r = 1.4$), within the first layers on the $\alpha = \pm 1$ surfaces. (d) Distribution of polymer-wall interaction energies, for the $\alpha = \pm 1$ systems.
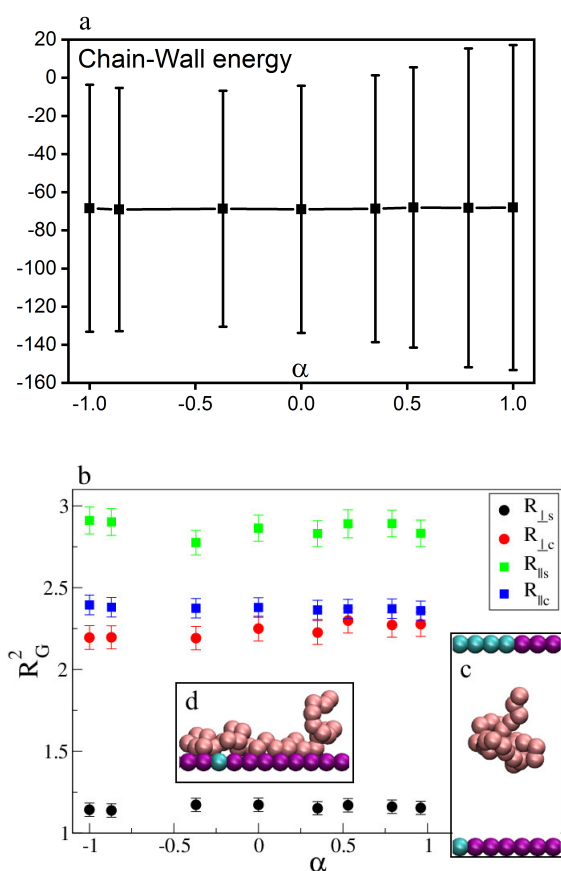
Fig. 5 Average structural properties. (a) α-dependence of the average polymer-wall interaction energy. Error bars correspond to the standard deviations of the associated distributions, like those shown in Fig.4d for the two extreme α values. (b) α-dependence of the perpendicular and parallel components of the chains' gyration radii, $R^2_{\perp c}, R^2_{\|c}$ and $R^2_{\perp s}, R^2_{\|s}$, as measured in the layers at the center or close to the surfaces. Snapshots of typical chain conformations in the two layers are shown in panel (c) and (d), respectively.

position have a pronounced effect. Heterogeneities in the polymer dynamics are dramatically enhanced when the surfaces are decorated with patches at least comparable to the chain size. In this case, in addition to a generic increase in the longest relaxation time, there is a clear decoupling between it and the diffusion coefficient. We emphasize that DH and the related decoupling occurring in our systems are not a trivial extension of the scenario emerging in glassy systems. First, in glass forming systems DHs appear on changing a thermodynamic control parameter (e.g., the temperature or the volume fraction), whereas here they are triggered by varying an "external" structural parameter (the energy topography and morphology of the walls). Second, DHs in our systems are localized near the walls, instead of being distributed within the whole sample volume. Notwithstanding DH localization, the decoupling involves quantities that refers to the system as whole (i.e. diffusion coefficient and relaxation time).

Several previous works studied thin and confined polymer films and might share inspiring similarities with the phenomena emerging in our systems. See Refs.[12,13,23,27,55–59], just to cite a few

examples. However, most of these contributions focused on systems cooled down to a glassy state and investigated the extent to which confinements interferes with the underlying glassy dynamics. Conversely, here we have consider a simple, non-supercooled polymer melt. When the confining surfaces are heterogeneous, novel dynamical features may appear even in the absence of readily detectable structural changes within the polymer melt. Their experimental identification seems very challenging, but it might become possible by the ingenuous application of novel characterization methods on carefully prepared systems. Patterned or block copolymer surfaces may be used as model substrates with well-defined morphologies and correlation lengths.[60] For example, recent experiments on fluorescent probes immobilized at block copolymer interfaces allowed the determination of local T_g's with nanometric resolution and their correlation with compositional profiles.[61]

As a final note, we point out that we have looked at the properties of weakly confined systems, as the middle of the slab can accomodate unperturbed polymer chains with bulk-like behavior. In the future, we plan to look at strongly confined systems, with longer chains capable of forming wall-to-wall bridges and entanglements. In addition to their equilibrium structure and dynamics, it should be interesting to consider the behavior of these systems undergoing flow or mechanical deformation.

Conflicts of interest

There are no conflicts to declare.

Acknowledgements

Notes and references

1 A. V. Pocius, *Adhesion and Adhesives Technology, 3rd edition*, Hanser Verlag, Munich, 2012.

2 J. Gao, W. D. Luedtke, D. Gourdon, M. Ruths, J. N. Israelachvili and U. Landman, *The Journal of Physical Chemistry B*, 2004, **108**, 3410–3425.

3 B. N. Persson, *Sliding friction: physical principles and applications*, Springer Science & Business Media, 2013.

4 L. Bocquet and E. Charlaix, *Chemical Society Reviews*, 2010, **39**, 1073–1095.

5 S. Granick, Y. Zhu and H. Lee, *Nature materials*, 2003, **2**, 221.

6 B. Zuo, M. Inutsuka, D. Kawaguchi, X. Wang and K. Tanaka, *Macromolecules*, 2018, **51**, 2180–2186.

7 T. A. Vilgis, G. Heinrich and M. Klüppel, *Reinforcement of polymer nano-composites: theory, experiments and applications*, Cambridge University Press, 2009.

8 J. Jancar, J. Douglas, F. W. Starr, S. Kumar, P. Cassagnau,

A. Lesser, S. S. Sternstein and M. Buehler, *Polymer*, 2010, **51**, 3321–3343.

9 S. Cheng, B. Carroll, V. Bocharova, J.-M. Carrillo, B. G. Sumpter and A. P. Sokolov, *The Journal of Chemical Physics*, 2017, **146**, 203201.

10 E. N. Skountzos, A. Anastassiou, V. G. Mavrantzas and D. N. Theodorou, *Macromolecules*, 2014, **47**, 8072–8088.

11 H. K. Nguyen, X. Liang, M. Ito and K. Nakajima, *Macromolecules*, 2018.

12 S. Napolitano, E. Glynos and N. B. Tito, *Reports on Progress in Physics*, 2017, **80**, 036602.

13 S. Napolitano and M. Wübbenhorst, *Nature communications*, 2011, **2**, 260.

14 A. V. Lyulin, N. K. Balabaev, A. R. Baljon, G. Mendoza, C. W. Frank and D. Y. Yoon, *The Journal of chemical physics*, 2017, **146**, 203314.

15 C. C. Lin, E. Parrish and R. J. Composto, *Macromolecules*, 2016, **49**, 5755–5772.

16 J. Choi, N. Clarke, K. I. Winey and R. J. Composto, *Macromolecules*, 2017, **50**, 3038–3042.

17 J. N. Israelachvili, *Intermolecular and surface forces*, Academic press, 2011.

18 J.-B. Donnet, R. C. Bandal and M.-J. Wang, *Carbon black: science and technology, 2nd edition*, Marcel Dekker, 1993.

19 A. Schröder, M. Klüppel and R. H. Schuster, *Macromolecular Materials and Engineering*, 2007, **292**, 885–916.

20 A. Baumgärtner and M. Muthukumar, *The Journal of Chemical Physics*, 1991, **94**, 4062.

21 T. A. Vilgis, *Polymer*, 2005, **46**, 4223–4229.

22 A. Yethiraj, *Advances in Chemical Physics*, 2002, **121**, 89–140.

23 G. D. Smith, D. Bedrov and O. Borodin, *Physical review letters*, 2003, **90**, 226103.

24 K. A. Smith, M. Vladkov and J.-L. Barrat, *Macromolecules*, 2005, **38**, 571–580.

25 A. De Virgiliis, A. Milchev, V. G. Rostiashvili and T. A. Vilgis, *The European physical journal. E, Soft matter*, 2012, **35**, 97.

26 V. A. Froltsov, M. Klüppel and G. Raos, *Physical Review E*, 2012, **86**, 041801/1–10.

27 J. Baschnagel and F. Varnik, *Journal of Physics: Condensed Matter*, 2005, **17**, R851.

28 D. N. Theodorou, G. G. Vogiatzis and G. Kritikos, *Macromolecules*, 2014, **47**, 6964–6981.

29 G. Raos and T. J. Sluckin, *Macromolecular Theory and Simulations*, 2013, **22**, 225–237.

30 G. Raos and J. Idé, *ACS Macro Letters*, 2014, **3**, 721–726.

31 R. Pastore and G. Raos, *Soft matter*, 2015, **11**, 8083–8091.

32 B. Wang, J. Kuo, S. C. Bae and S. Granick, *Nature materials*, 2012, **11**, 481.

33 M. Doi and S. F. Edwards, *The theory of polymer dynamics*, Oxford University Press, 1988.

34 J. T. Kalathi, S. K. Kumar, M. Rubinstein and G. S. Grest, *Macromolecules*, 2014, **47**, 6925–6931.

35 S. J. Marrink, H. J. Risselada, S. Yefimov, D. P. Tieleman and A. H. de Vries, *The Journal of Physical Chemistry B*, 2007, **111**, 7812–24.

36 M. E. Mackura and D. S. Simmons, *Journal of Polymer Science Part B: Polymer Physics*, 2014, **52**, 134–140.

37 K. Kremer and G. S. Grest, *The Journal of Chemical Physics*, 1990, **92**, 5057–5086.

38 S. Plimpton, *Journal of computational physics*, 1995, **117**, 1–19.

39 K. Huang, *Statistical Mechanics, 2nd edition*, John Wiley & Sons, New York, 1987.

40 B. E. Warren, *X-ray Diffraction*, Dover Publications, 1990.

41 A. Cavagna, *Physics Reports*, 2009, **476**, 51–124.

42 L. Berthier and G. Biroli, *Reviews of Modern Physics*, 2011, **83**, 587.

43 R. Pastore, G. Pesce, A. Sasso and M. Pica Ciamarra, *The Journal of Physical Chemistry Letters*, 2017, **8**, 1562–1568.

44 R. Pastore, G. Pesce and M. Caggioni, *Scientific Reports*, 2017, **7**, 43496.

45 R. Pastore, M. Pica Ciamarra and A. Coniglio, *Fractals*, 2013, **21**, 1350021.

46 E. Rössler, *Physical review letters*, 1990, **65**, 1595.

47 P. G. Debenedetti and F. H. Stillinger, *Nature*, 2001, **410**, 259.

48 J.-H. Hung, J. H. Mangalara and D. S. Simmons, *Macromolecules*, 2018, **51**, 2887–2898.

49 L. Berthier, G. Biroli, J.-P. Bouchaud, L. Cipelletti and W. van Saarloos, *Dynamical heterogeneities in glasses, colloids, and granular media*, OUP Oxford, 2011, vol. 150.

50 C. Bennemann, C. Donati, J. Baschnagel and S. C. Glotzer, *Nature*, 1999, **399**, 246.

51 J. Helfferich, J. Brisch, H. Meyer, O. Benzerara, F. Ziebert, J. Farago and J. Baschnagel, *The European Physical Journal E*, 2018, **41**, 71.

52 M. T. Cicerone and M. D. Ediger, *The Journal of chemical physics*, 1996, **104**, 7210–7218.

53 R. Pastore, A. Coniglio, A. de Candia, A. Fierro and M. Pica Ciamarra, *Journal of Statistical Mechanics: Theory and Experiment*, 2016, **2016**, 054050.

54 C. P. Royall and S. R. Williams, *Physics Reports*, 2015, **560**, 1–75.

55 P. Z. Hanakata, J. F. Douglas and F. W. Starr, *Nature communications*, 2014, **5**, 4163.

56 M. Alcoutlabi and G. B. McKenna, *Journal of Physics: Condensed Matter*, 2005, **17**, R461.

57 J. Torres, P. Nealey and J. De Pablo, *Physical Review Letters*, 2000, **85**, 3221.

58 C. J. Ellison and J. M. Torkelson, *Nature materials*, 2003, **2**, 695.

59 R. D. Priestley, C. J. Ellison, L. J. Broadbelt and J. M. Torkelson, *Science*, 2005, **309**, 456–459.

60 H.-C. Kim, S.-M. Park and W. D. Hinsberg, *Chemical reviews*, 2009, **110**, 146–177.

61 D. Christie, R. A. Register and R. D. Priestley, *ACS central science*, 2018, **4**, 504–511.